





ORIGINAL ARTICLE

Nucleic acid-triggered tumoral immunity propagates pH-selective therapeutic antibodies through tumor-driven epitope spreading

Genta Furuya¹ | Hiroto Katoh¹  | Shinichiro Atsumi¹ | Itaru Hashimoto¹ | Daisuke Komura¹  | Ryo Hatanaka² | Shogo Senga² | Shuto Hayashi¹ | Shoji Akita² | Hirofumi Matsumura² | Akihiro Miura² | Hideaki Mita¹ | Makoto Nakakido³ | Satoru Nagatoishi³ | Akira Sugiyama⁴  | Ryohei Suzuki¹ | Hiroki Konishi¹ | Asami Yamamoto¹ | Hiroyuki Abe⁵ | Nobuyoshi Hiraoka⁶  | Kazunori Aoki⁷  | Yasumasa Kato⁸ | Yasuyuki Seto⁹ | Chihoko Yoshimura² | Kazutaka Miyadera² | Kouhei Tsumoto³ | Tetsuo Ushiku⁵ | Shumpei Ishikawa¹

¹Department of Preventive medicine, Graduate School of Medicine, The University of Tokyo, Tokyo, Japan

²Discovery and Preclinical Research Division, Taiho Pharmaceutical Co., Ltd., Ibaraki, Japan

³Laboratory of Medical Proteomics, Institute of Medical Science, The University of Tokyo, Tokyo, Japan

⁴Laboratory of Systems Biology and Medicine, Research Center for Advanced Science and Technology, The University of Tokyo, Tokyo, Japan

⁵Department of Pathology, Graduate School of Medicine, The University of Tokyo, Tokyo, Japan

⁶Department of Analytical Pathology, National Cancer Center Research Institute, Tokyo, Japan

⁷Division of Molecular and Cellular Medicine, National Cancer Center Research Institute, Tokyo, Japan

⁸Department of Oral Function and Molecular Biology, Ohu University School of Dentistry, Fukushima, Japan

⁹Department of Gastrointestinal Surgery, Graduate School of Medicine, The University of Tokyo, Tokyo, Japan

Correspondence

Hiroto Katoh and Shumpei Ishikawa,
Department of Preventive Medicine,
Graduate School of Medicine, The
University of Tokyo, 7-3-1 Hongo,
Bunkyo-ku, Tokyo, 113-0033 Japan.
Emails: hkat-prm@m.u-tokyo.ac.jp;
ishum-prm@m.u-tokyo.ac.jp

Funding information

Japan Agency for Medical Research and
Development, Grant/Award Number:
JP22ak0101096 and JP22am0401010;
Japan Society for the Promotion
of Science, Grant/Award Number:
19H01032; Mizutani Foundation for
Glycoscience; Taiho Pharmaceutical

Abstract

Important roles of humoral tumor immunity are often pointed out; however, precise profiles of dominant antigens and developmental mechanisms remain elusive. We systematically investigated the humoral antigens of dominant intratumor immunoglobulin clones found in human cancers. We found that approximately half of the corresponding antigens were restricted to strongly and densely negatively charged polymers, resulting in simultaneous reactivities of the antibodies to both densely sulfated glycosaminoglycans (dsGAGs) and nucleic acids (NAs). These anti-dsGAG/NA antibodies matured and expanded via intratumoral immunological driving force of innate immunity via NAs. These human cancer-derived antibodies exhibited acidic pH-selective affinity across both antigens and showed specific reactivity to diverse spectrums of human tumor cells. The antibody-drug conjugate exerted therapeutic effects against multiple cancers in vivo by targeting cell surface dsGAG antigens. This study reveals that intratumoral immunological reactions propagate tumor-oriented

This is an open access article under the terms of the [Creative Commons Attribution-NonCommercial](https://creativecommons.org/licenses/by-nc/4.0/) License, which permits use, distribution and reproduction in any medium, provided the original work is properly cited and is not used for commercial purposes.

© 2022 The Authors. *Cancer Science* published by John Wiley & Sons Australia, Ltd on behalf of Japanese Cancer Association.

immunoglobulin clones and demonstrates a new therapeutic modality for the universal treatment of human malignancies.

KEYWORDS

(14) characteristics and pathology of human cancer, humoral immunity, immune repertoire, pH-selective antibody, sulfated glycosaminoglycan, tumor-infiltrating B cell

1 | INTRODUCTION

Cellular immunity, including cytotoxic T cell biology, has been attracting attention due to the clinical successes of immune checkpoint blockade therapies.¹ Meanwhile, important roles for humoral tumor immunity have also been pointed out,^{2,3} and studies on humoral tumor immunity revealed various important aspects on tumor-infiltrating B/plasma cells.^{4–11} However, the precise functions of B cells in tumor environments remain elusive, due in part to the lack of identification of antigen (Ag) repertoires recognized by tumor-infiltrating B/plasma cells.

Identifying the Ags of tumor-infiltrating B/plasma cells contributes to the elucidation of fundamental biology of humoral tumor immunity,^{12,13} including immunological driving forces, mechanisms or origins, and therapeutic applicability. Some studies reported possible Ags of tumor-infiltrating B/plasma cells,^{14,15} in which overexpressed proteins and cancer testis Ags were identified as humoral tumor Ags. However, it is still not clarified whether such tumor-associated Ags constitute the major fractions or minor components in the milieu of tumor-associated humoral immunity.

We previously clarified a global profile of immune receptor repertoires of tumor-infiltrating lymphocytes in human cancers, discovering a large number of tumor-specific dominant B/plasma cell clones.^{16,17} It was found that multiple of such clones commonly recognized sulfated glycosaminoglycan (GAG) or focal adhesion ribonucleoprotein (RNP) complex proteins.^{16,17} Thus, a hypothesis has been achieved that anti-GAG and anti-RNP constitute a significant portion of humoral tumor immunity. It was warranted to investigate the immunological driving forces for the Abs to dominate in tumor environments as well as their therapeutic applicability for human malignancies.

Glycosaminoglycans are linear polysaccharide glycans composed of repeated disaccharides and classified into five groups: hyaluronic acid, heparan sulfate (HS), chondroitin sulfate, dermatan sulfate, and keratan sulfate.¹⁸ GAG is well known to interact with and condensate various growth factors on tumor cell surfaces.¹⁹ Each disaccharide harbors various degrees of sulfonate group modifications; therefore, GAG polysaccharides consist of almost infinite diversity in chemical structures. The high frequency of tumor-specific anti-GAG humoral

immunity implies the existence of tumor-specific GAG structures; however, the sulfation patterns in the GAG polysaccharides are difficult to determine.^{18,20,21}

In this study, we investigated detailed chemical structures of the GAG epitopes corresponding to the tumor-specific dominant anti-GAG Abs, as well as the immunological driving forces for the emergence/development of such immunoglobulin (Ig) clones, specifically in human cancer environments. Eventually, we exhibit the highly efficient and universal therapeutic applicability of such anti-GAG Abs found in human cancers against wide spectrums of malignancies *in vivo*.

2 | MATERIALS AND METHODS

2.1 | Human samples

This study was approved by the institutional review boards of the University of Tokyo, Tokyo Medical and Dental University, and National Cancer Center Hospital, Tokyo, Japan. A total of 102 and 27 specimens of gastric and pancreatic carcinomas, respectively, were obtained with informed consent. Tissue microarrays were constructed with the approval of the University of Tokyo. Details are described in Methods S1.

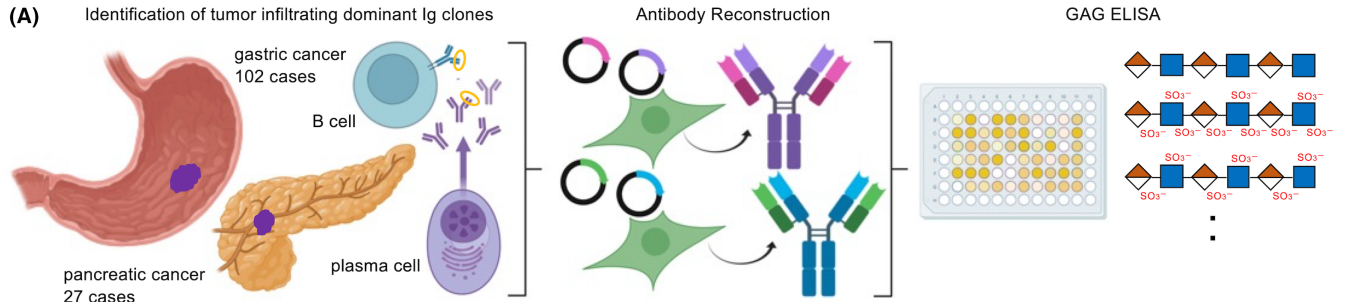
2.2 | Mice

The animal studies were approved by Taiho Pharmaceutical Co., Ltd. and the University of Tokyo, where appropriate, as described in Methods S1.

2.3 | Repertoire sequencing and reconstruction of antibodies

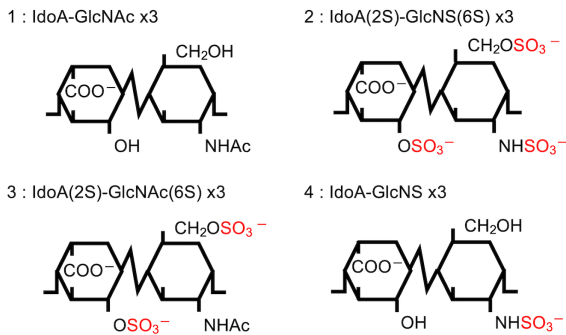
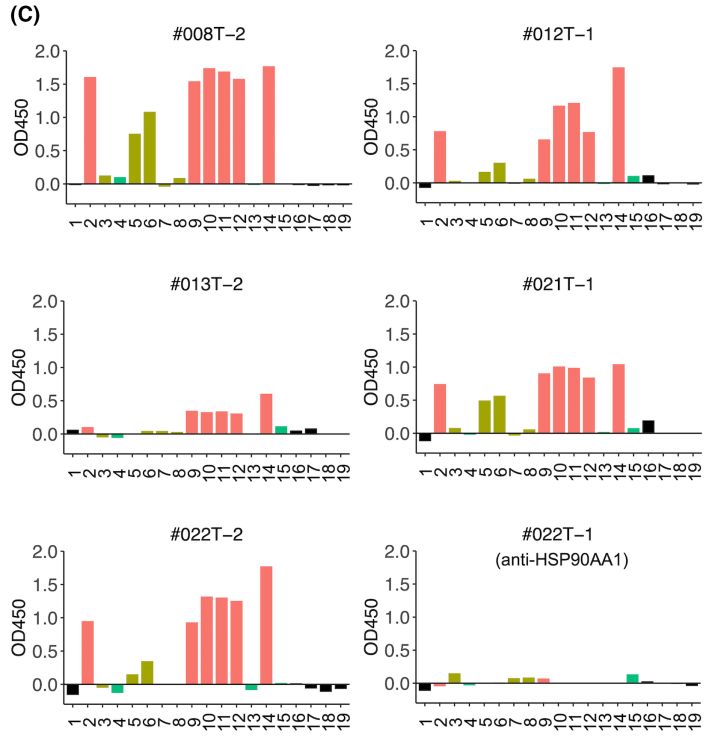
Repertoire sequencing and the reconstruction of the tumor-infiltrating dominant clones as human IgG1 were performed as described previously^{16,17} (see Methods S1). The Ig repertoire sequence data of gastric cancers are deposited in JGAS00000000242.

FIGURE 1 Identification of tumor-infiltrating dominant anti-densely sulfated glycosaminoglycan (dsGAG) immunoglobulin (Ig) clones. A, Workflow of the identification of antigens (Ags) for tumor-infiltrating dominant clones. B, GAG and glycan Ags in GAG ELISA are shown with their densities of sulfation. C, Results of GAG ELISA of high-affinity anti-dsGAG clones and an anti-protein clone as a negative control (#022T-1, anti-HSP90AA1). D, Amino acid sequences of the heavy chain CDR3s of high-affinity anti-dsGAG clones (red: acidic, blue: basic, green: neutral [hydrophilic], and black: hydrophobic). E, F The mean fluorescent intensities (MFIs) of high-affinity anti-dsGAG clones to HGC27 and NUGC3 with/without heparinase I + III digestions (HSase) (E) and siRNA-mediated knockdown of EXT1/2 (siEXT1&2) (F) ($n = 3$). Bars and error bars represent the mean and SD, respectively.



(B)

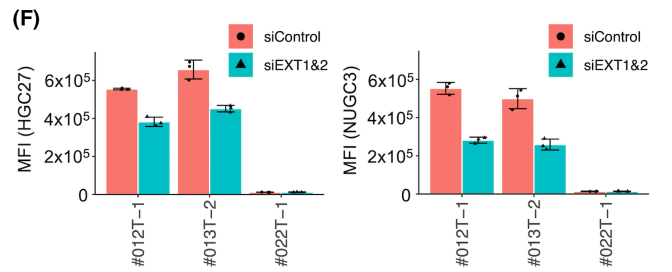
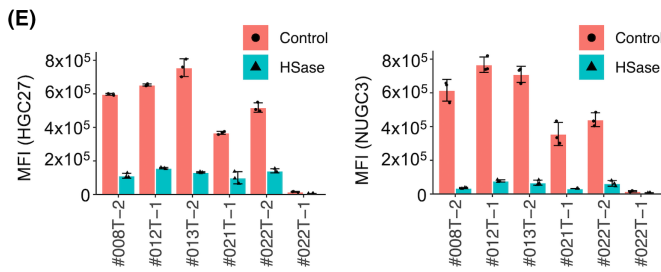
No	antigen	sulfation density
1	Oligomer 1	—
2	Oligomer 2	+++
3	Oligomer 3	++
4	Oligomer 4	+
5	2-O-Desulfated Heparin oligo dp6	++
6	6-O-Desulfated Heparin oligo dp6	++
7	N-Desulfated Heparin oligo dp6	++
8	N-Desulfated re N-Acetylated Heparin oligo dp6	++
9	Hexasaccharide, dp6	+++
10	Dodecasaccharide, dp12	+++
11	Heparin, dp18	+++
12	Sodium Heparin from porcine intestinal mucosa	+++
13	Sodium Chondroitin Sulfate	+
14	Over Sulfated Chondroitine Sulfate (OSCS)	+++
15	Sodium Dermatan Sulfate	+
16	Hyaluronic Acid from Cockscomb	—
17	Hyaluronic Acid oligo dp6	—
18	Cellopentaose	—
19	Sialyl Lewis X-Lactose	—



(D)

anti-dsGAG Ig clones (high affinity)

ID	H-CDR3
#008T-2	ARGPELLSQNYYYYGMDV
#012T-1	ASSQAYIDVSGGPVNN
#013T-2	AKGLLPSLPYGMDV
#021T-1	ARAESYDSDSHYYNGLDV
#022T-2	VREDSSSWHPGRYIQL



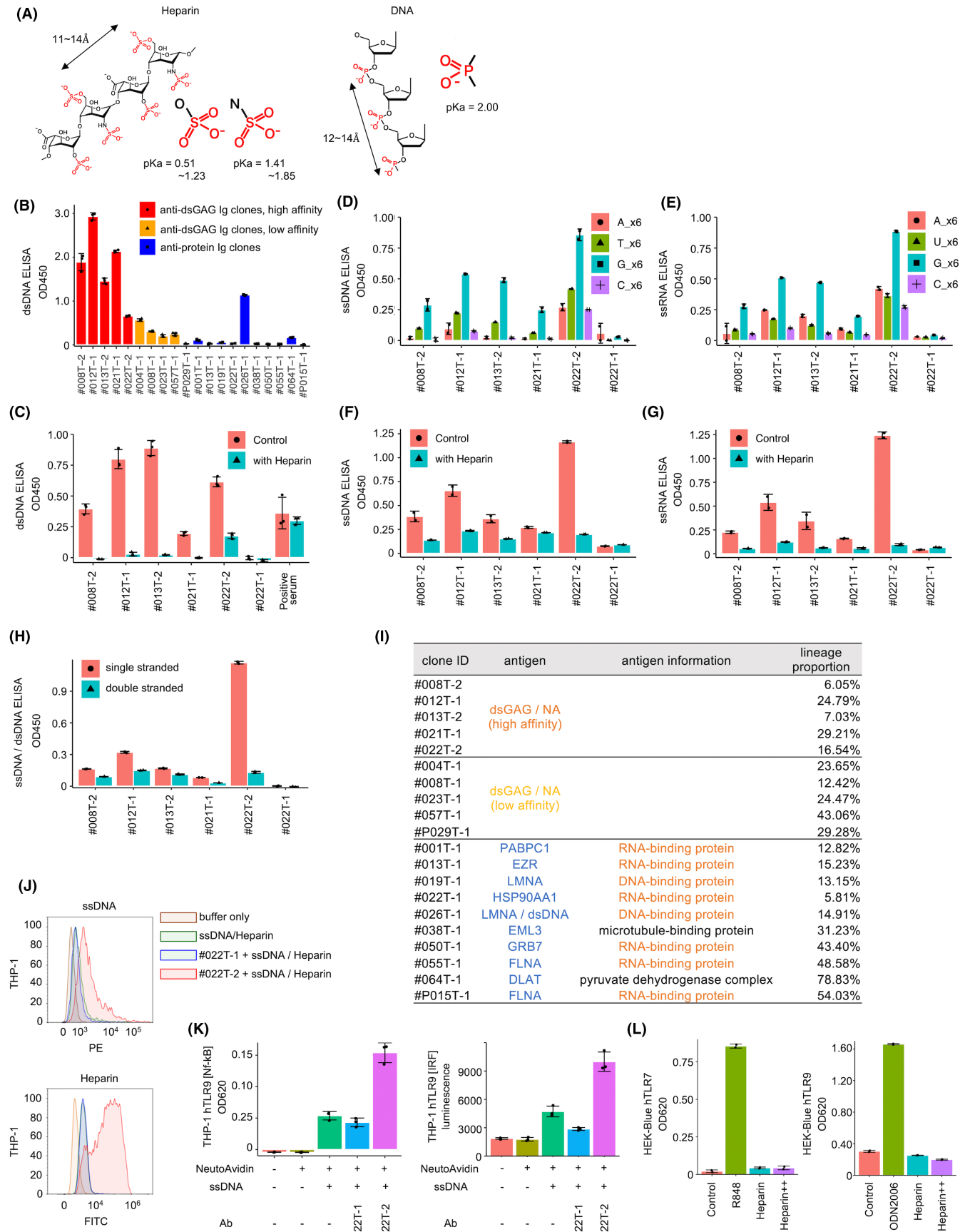


FIGURE 2 Dual reactivity of anti-densely sulfated glycosaminoglycan (anti-dsGAG) clones to nucleic acids (NAs). A, Schematic diagram of heparin (dsGAG) and phosphodiester backbone of DNA. B, double-stranded DNA (dsDNA) ELISA signals of tumor-infiltrating dominant clones ($n = 3$). C, dsDNA ELISA signals of the high-affinity anti-dsGAG clones with/without coincubation of Heparin ($n = 3$). Serum from autoimmune patients were used as a control. D, E, ELISA signals of high-affinity anti-dsGAG clones to 6-mer oligos of single-stranded DNA (ssDNA) (D) and ssRNA (E) ($n = 2$). F, G, Signals of ssDNA (F) and ssRNA (G) ELISAs with/without coincubation of heparin ($n = 2$). H, dsDNA and ssDNA ELISAs were performed in parallel for high-affinity anti-dsGAG clones ($n = 2$). I, Defined antigens (Ags) for 20 out of 30 reconstructed tumor-infiltrating dominant immunoglobulin (Ig) clones with the information of their proportions of lineage sizes in the repertoires in each tumor. J, Internalizations of phycoerythrin (PE)-ssDNA and FITC-heparin with/without coincubations of #022T-2 were evaluated by flow cytometry (FC) using THP-1 cell. K, TLR9 signals in THP-1 cell with/without coincubations of ssDNA and/or #022T-2 were evaluated by Nf-kB and IRF reporter systems ($n = 3$). L, Activations of TLR7/9 in HEK-Blue cells were evaluated with/without coincubation of R848 (hTLR7 agonist), ODN2006 (hTLR9 agonist), or heparin ($n = 2$). Bars and error bars represent the mean and SD, respectively.

2.4 | Biochemical and histopathological experiments

Enzyme-linked immunosorbent assay (ELISA), flow cytometry (FC), RNA in situ hybridization (RNA-ISH), measurements of TLR and NF-kB signals, immunohistochemistry (IHC), and immunocytochemistry (ICC) were performed as described in Methods S1.

2.5 | Definition of tumor-associated tertiary lymphoid structure (tTLS) score

Tumor sections of hematoxylin and eosin (HE)-stained gastric and pancreatic cancers were examined under a microscope. The abundance of tTLS was evaluated as described in Methods S1.

2.6 | Construction of antibody-drug conjugate (ADC)

An ADC based on an anti-dsGAG/nucleic acid (NA) clone #022T-2, named #022T-2m-VC-PAB-MMAE, was constructed as described in Methods S1.

2.7 | Supplementary experiments

Other methods of experiments in this study are fully described in Methods S1, including those for differentially expressed gene analysis, quantitative reverse-transcription PCR, immunoprecipitation, mass spectrometry, immunoblot, competitive assays of growth factors, Transwell assays, ADCC reporter assays, dual-luciferase reporter assays, MTT assays, cell viability assays, and surface plasmon resonance (SPR).

3 | RESULTS

3.1 | Densely sulfated GAG (dsGAG) is the major and shared Ag of tumor-infiltrating dominant Ig clones

As we previously reported, sulfated GAG is the major humoral Ag of tumor-infiltrating B/plasma cells in human gastric cancer environments.¹⁷ To determine the precise chemical structures of the sulfated

GAG Ags, we used a GAG library covering diverse sulfation patterns (Figure 1A,B). We performed GAG ELISA using 30 tumor-infiltrating dominant Ig clones identified from the repertoire sequencing of 102 gastric cancers^{16,17} and additional 27 pancreatic cancers (Figure 1A). Five high-affinity and five low-affinity anti-sulfated GAG clones, including those previously reported,¹⁷ were identified (Figure 1C; Figure S1B,C). It was revealed that the reactivities of the clones to sulfated GAGs were proportional to sulfonate densities of GAG epitopes (Figure 1C). Therefore, it is concluded that the specific and common Ag of anti-sulfated GAG clones found in cancer environments is the dsGAG. Although five high-affinity anti-dsGAG clones exhibited similar reactive patterns to the dsGAG epitopes, little similarities were observed in their complementarity-determining region 3 (CDR3) (Figure 1D).

Heparin, a highly sulfated form of HS, is the major form of dsGAG in human body.^{18,22} The anti-dsGAG nature of the Ig clones was confirmed by FC targeting cell surface HS on human cancer cells, in which substantial reductions of FC signals of the anti-dsGAG clones were observed under heparinase I+III digestion (Figure 1E) and EXT1/EXT2 knockdown, two essential glycosyltransferases for HS synthesis (Figure 1F). The knockdown efficacies of EXT1 and EXT2 were confirmed by quantitative PCR (Figure S1D). It was concluded that the anti-dsGAG clones are functional Abs to cell surface dsGAG of cancer cells.

We also searched for protein Ags for the 30 dominant Ig clones found in human gastric or pancreatic cancer environments, discovering 10 protein Ags, including those previously reported (Figure 2; Figure S1C).^{16,17} The remaining 10 clones were still orphan Igs due to possible difficulties in technical conditioning. Therefore, it was surprisingly shown that half (10/20) of the dominant clones with defined Ags, in human tumor environments, commonly recognized dsGAG.

3.2 | Anti-dsGAG Ig clones are dual reactive to NAs

The GAG ELISA of the anti-dsGAG clones showed signals in a wide range of sulfated GAGs (Figure 1C). This broad reactivity to negatively charged GAGs made us hypothesize that anti-dsGAG clones are also reactive to other negatively charged polyanions (Figure S2A).²³ Among the polyanions, NA was considered the most possible candidate as an Ag of the clones, based on its similarities

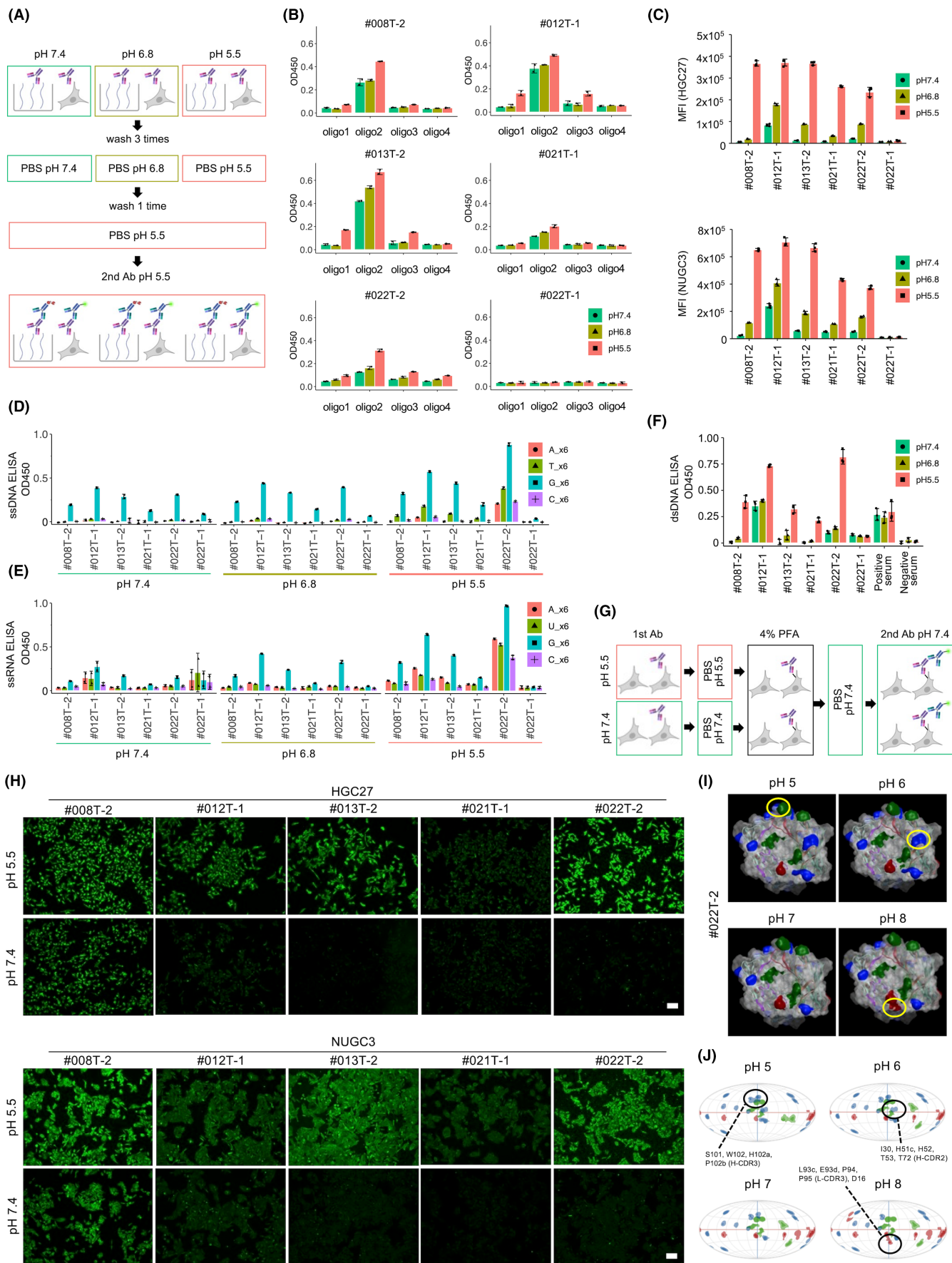


FIGURE 3 The pH-selectively enhanced affinity of anti-densely sulfated glycosaminoglycan/nucleic acid (anti-dsGAG/NA) clones. A, Workflow of ELISA and flow cytometry (FC) under various pH. B, GAG ELISAs using synthesized GAG oligomers (Figure 1B) at various pH for five high-affinity anti-dsGAG/NA clones. C, Mean fluorescent intensities (MFIs) of FC signals of high-affinity anti-dsGAG/NA clones bound to HGC27 and NUGC3 under indicated pH ($n = 3$). D, E, ssDNA (D) and ssRNA (E) ELISA signals of high-affinity anti-dsGAG/NA clones under various pH ($n = 2$). F, dsDNA ELISA of high-affinity anti-dsGAG/NA clones under various pH ($n = 3$), together with anti-dsDNA(+) serum from autoimmune patients and anti-dsDNA(-) serum. G, Workflow of immunocytochemistry (ICC) in pH 7.4 or 5.5. H, ICC for HGC27 and NUGC3 using high-affinity anti-dsGAG/NA clones in pH 7.4 and 5.5. Scale bars indicate 100 μm . I, J, The 3D-plot (I) and 2D-plot (J) of the simulations of surface electrostatics of a high-affinity anti-dsGAG/NA clone #022T-2 using Molecular Operating Environment platform. Simulations were conducted thrice, and patches whose electrostatics changed more than once in CDR were marked with yellow (I) and black (J) circles. Surface patches with blue, red, and green represent positively charged, negatively charged, and hydrophobic patches, respectively.

with dsGAG in pKa of phosphodiester^{24,25} and structural pitches of negative charges (Figure 2A).

In double-stranded DNA (dsDNA) ELISA, the high-affinity anti-dsGAG clones showed stronger reactivity to dsDNA than other anti-protein clones (Figure 2B). The dsDNA ELISA signals were almost completely attenuated by heparin, indicating the shared binding sites of anti-dsGAG clones for dsDNA and dsGAG (Figure 2C). The single-stranded DNA (ssDNA) and ssRNA ELISAs also showed reactivity of the high-affinity anti-dsGAG clones, especially to (deoxy) guanosine (G_{x6}) (Figure 2D and E). These ELISA signals were also attenuated by heparin (Figure 2F,G), although the attenuation effects were milder in ssDNA ELISA (Figure 2F) than in dsDNA ELISA (Figure 2C). It is suggested that the anti-dsGAG clones bind more preferably to single stranded polyanions, which are ssDNA, ssRNA, and dsGAG, presumably due to their biochemical and structural similarities. Preferable bindings of the anti-dsGAG clones to ssDNA rather than dsDNA were confirmed in an ELISA where their bindings were directly compared in parallel (Figure 2H). SPR analysis confirmed the binding of #022T-2 to ssDNA (Figure S2B). These data show that these tumor-infiltrating dominant clones are dual reactive to dsGAG and NAs.

As mentioned above, 10 protein Ags were identified among 30 tumor-infiltrating dominant clones from gastric and pancreatic cancers (Figure 2I; Figure S2C). Most, if not all, of these protein Ags were either DNA- or RNA-binding proteins (Figure 2I). Thus, at least 60.0% (18/30) of the tumor-infiltrating dominant clones, including both anti-dsGAG and anti-protein clones, react to NAs. NA is an established ligand and a stimulator of innate immune system in various immune cells, including B cells^{26,27} (Figure S2D,E). Among the known key players of NA-associated innate immunity, TLR7/9 are the best-fit models to be investigated based on the preferred reactivities of the clones to G-enriched and single-stranded NAs (Figure 1; Figure S2D). Using THP-1 human monocytic cell, it was shown that both ssDNA and heparin were internalized into cellular components with high-affinity anti-dsGAG/NA clone (#022T-2) (Figure 2J), confirming the physiological function of anti-dsGAG/NA clones. Under such condition, TLR9 signaling was drastically induced by ssDNA (Figure 2K). On the contrary, heparin could not induce either TLR7 or 9 signaling in HEK293 reporter (Figure 2L).

Taken together, tumor-associated humoral immunity was highly skewed to the anti-NA immunity, most likely through the activation

of the innate NA-TLR axis, which induced the emergences of highly dominant milieu of anti-dsGAG/NA and anti-NA-associated protein clones in tumors.

3.3 | Affinity of anti-dsGAG/NA Ig clones is acidic pH selective

The dual reactivity of the anti-dsGAG/NA clones to dsGAG/NA polyanions suggested that conditions under strong negative charges could achieve optimal binding. It is well known that tumor microenvironments exhibit acidic pH,²⁸⁻³⁰ as low as 5.5-6.8.³¹⁻³³ We hypothesized that anti-dsGAG/NA clones found in tumor environments would exhibit enhanced affinity to dsGAG/NA Ags under lower pH.

We conducted GAG ELISA in various pH conditions (pH 7.4, 6.8, and 5.5), revealing that ELISA signals of the high-affinity anti-dsGAG/NA clones, more specifically that of oligomer-2, showed pH dependency (Figure 3B). FC of anti-dsGAG/NA clones on human cancer cell lines showed drastic enhancements of signals in lower pH (Figure 3C). This acidic pH-dependent enhancement of the binding of anti-dsGAG/NA clones was also confirmed for ssDNA/ssRNA ELISAs (Figure 3D,E). In the dsDNA ELISA, the signals of anti-dsGAG/NA clones also exhibited pH dependency, while such pH dependency was negligible in serum from autoimmune disease patients (Figure 3F), indicating that anti-dsDNA Abs in autoimmunity and tumor immunity harbor different properties. ICC of human cancer cells also showed augmented signals of anti-dsGAG/NA clones in acidic pH (Figure 3G,H). Low-affinity anti-dsGAG/NA clones also showed, although vague, acidic pH selectivity (Figure S3A,B). Trastuzumab did not show acidic pH selectivity (Figure S3C) as reported,³⁴ supporting our conclusion that anti-dsGAG/NA clones found in tumor environments specifically exhibit characteristic pH dependency.

In silico pH titration analysis of the CDR of a high-affinity anti-dsGAG/NA clone #022T-2 showed that a negative-charged surface patch and two positive-charged surface patches disappeared and appeared, respectively, with the decrease in pH (Figure 3I). Most of the pH-dependent changes of surface electrostatics were detected in CDRs or neighboring regions (Figure 3J). Similar results were also observed in other high-affinity anti-dsGAG/NA clones,

such as #021T-1 and #008T-2 (Figure S3D). Some of these patches contained histidine (pKa of side chain: around 6.0), compatible with previous reports showing acidic pH-selective histidine-associated

protein binding.^{34–38} Dynamic and localized electrostatic changes in CDRs were the most likely mechanism of the acidic pH selectivity of the anti-dsGAG/NA clones.

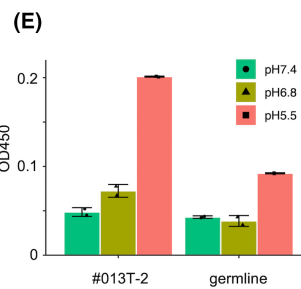
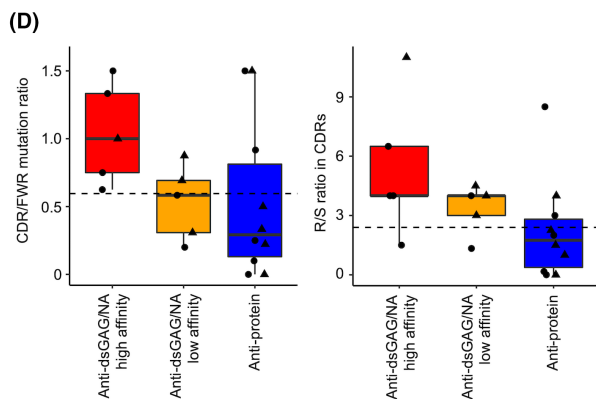
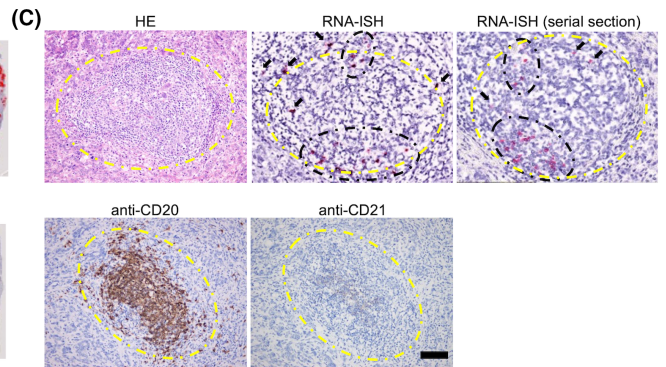
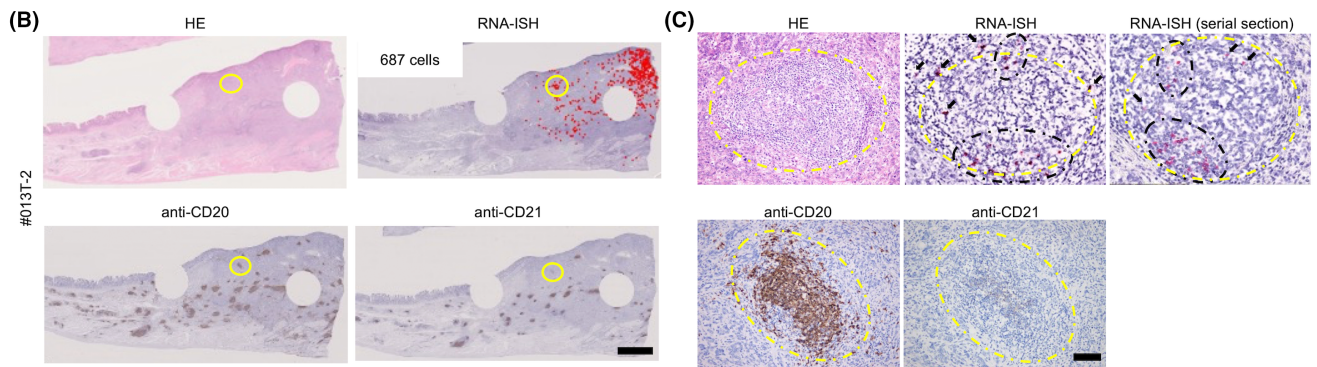
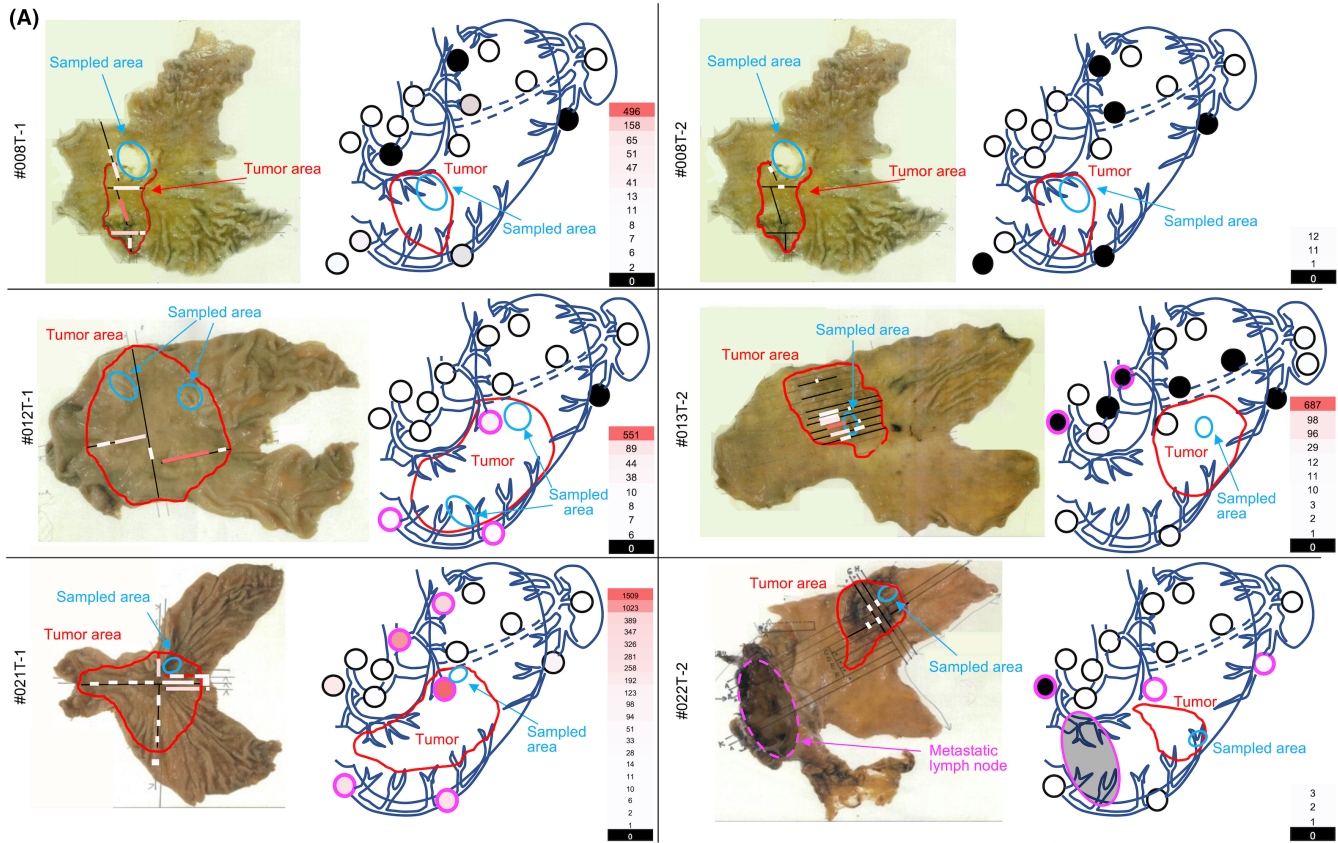


FIGURE 4 Distribution and maturation of anti-densely sulfated glycosaminoglycan/nucleic acid (anti-dsGAG/NA) clones in tumor environments. A, RNA in situ hybridization (RNA-ISH) targeting specific H-CDR3 sequences on the corresponding clinical cancer specimens. For each anti-dsGAG/NA clone, the distributions of cells with positive RNA-ISH signals in gastric tumors and regional lymph nodes (LNs) are summarized. Bold colored lines in tumor areas in left panels and colors of LNs in right panels indicate the numbers of positive cells as indicated by color scales on the right side. LNs with magenta circles indicate tumor metastases. B, C, Representative images of RNA-ISH of #013T-2, as well as immunohistochemistry (IHC) using anti-CD20 and anti-CD21 Abs. High-power images focusing on the yellow-circled areas of (B) are shown in (C). Dashed yellow circle indicates tumor-associated tertiary lymphoid structure (tTLS). Scale bars indicate 2.5 mm (B) and 100 μ m (C). D, The mutation ratio of CDRs to framework regions (CDR/FWR) and the ratio of replacement mutations to silent mutations (R/S ratio) in CDR of anti-dsGAG/NA clones and anti-protein clones. Each dot represents an immunoglobulin (Ig) clone, and round and triangle shapes represent whether the clones were derived from tTLS-high or tTLS-low cases, respectively. Dashed horizontal lines represent the means of the CDR/FWR mutation ratio and R/S ratio in CDR of the top 30 clones (Figure S4F,G). E, ssDNA ELISA using #013T-2, and its germline clone (Figure S4H), under various pH ($n = 2$).

3.4 | Local tumor microenvironment is the source of anti-dsGAG/NA Ig clones

To explore the origin of the anti-dsGAG/NA clones, we conducted RNA-ISH using probes specific to the CDR3s of heavy chains, to detect the distributions of specific anti-dsGAG/NA B/plasma cell clones. In both frozen and formalin-fixed paraffin-embedded (FFPE) clinical specimens, positive ISH signals of anti-dsGAG/NA clones were detected in the matched tumor samples (Figures S4A,B).

RNA-ISH was conducted on all the available FFPE sections of tumors and dissected lymph nodes (LNs). For most of the high-affinity anti-dsGAG/NA clones (#008T-1, #012T-1, #013T-2, and #021T-1), characteristically localized and gradient distributions of the plasma cell clones were observed with the highest existences in the primary tumor areas (Figure 4A). The more the distances from the tumor sites, the fewer the clones detected. Although only a few signals of #008T-2 and #022T-2 were detected in RNA-ISH, the tendency of the localized and gradient distribution patterns were observed (Figure 4A). Much fewer signals were detected in the dissected LNs than in the intratumoral regions in most cases, except for #021T-1. There were no localized distribution patterns along with the lymphatic distance of the LNs from the primary tumor sites, nor was the #021T-1 (Figure 4A). There were no associations between LN metastasis of tumors and the numbers of positive cells in LNs (Figure 4A). Additionally, positive ISH signals of #013T-2 plasma cell clone were detected in and around tumor-associated tTLSs within the primary tumor (Figure 4B,C).

The localized and gradient distribution patterns of the clones in the primary tumor sites, not in regional LNs, as well as the specific existences of the plasma cell clones in the tTLS within tumors indicated that the anti-dsGAG/NA clones were supplied from primary tumor microenvironments, not from regional tumor-draining LNs. Based on the possible link between the intratumor emergence of anti-dsGAG/NA clones and the existence of tTLSs within tumor microenvironments, we evaluated the associations between the tTLS abundance (assigned to each case histologically [Figure S4C–E]) and well-known indicators of positive selection bias of affinity maturation of B cell clones: the ratio of replacement mutations in CDRs to those in framework regions (FWRs) (CDR/FWR mutation ratio) and the ratio of replacement mutations to silent mutations in CDRs (R/S ratio in CDR).³⁹ Among the global IgG clones in tumors,

the tTLS scores and both CDR/FWR mutation ratio and R/S ratio in CDR were significantly correlated (Figure S4F,G). It is suggested that significant amounts of tumor-infiltrating IgG clones were matured through tTLS. The high-affinity anti-dsGAG/NA clones showed higher CDR/FWR mutation ratio and R/S ratio in CDR than the low-affinity anti-dsGAG/NA clones (Figure 4D). This result suggests that the high-affinity anti-dsGAG/NA clones acquired somatic hypermutations (SHMs) to mature and expand in tTLSs, being supported by the fact that most of the high-affinity anti-dsGAG/NA clones were discovered in tTLS-high tumors (Figure 4D). The reactivity of the germline variant of #013T-2 (Figure S4H) to NAs was substantially lower than that of affinity-matured #013T-2 (Figure 4E), revealing that SHMs contributed to the augmented affinity and signature pH selectivity of the #013T-2 clone.

As indicated above, the TLR-related innate immunity system possibly plays a role in the activation of anti-dsGAG/NA clones (Figure 2). It is noteworthy that the acquired immunity system through SHMs in tTLSs also works in the emergence of such clones. With reference to previous reports showing that TLR7/9 in B cells augmented the formation of germinal centers,^{40,41} our data suggest that the acidic pH conditions of tumor microenvironments and the tTLSs worked in concert with innate immunity to promote the expansion of the pH-selective anti-dsGAG/NA clones.

3.5 | Histological and cytological distributions of the Ags of anti-dsGAG/NA Ig clones

To investigate the distribution of the Ags of the anti-dsGAG/NA clones in cancers, IHC was conducted. This involved the use of #012T-1 and #013T-2 clones. To our surprise, universal and homogeneous positive IHC signals were detected in tumor cells of all the epithelial cancer types examined, both in the cytoplasm and on cell surfaces (Figure 5A). Nearly all cases of seven epithelial cancer types had positive cancer-specific staining (Figure S5A,B). Staining patterns and signal intensities of #012T-1 and #013T-2 clones were highly concordant with each other (Figure S5A,B), confirming that these anti-dsGAG/NA clones commonly reacted to the same Ags. In contrast, mesenchymal tumors such as osteosarcoma showed slight or negligible signals (Figure S5C). Positive signals in tumor cells were clearly nullified by heparin coinubation (Figure 5B,C; Figure S5D),

indicating that the tumor cells genuinely expressed the Ags corresponding to the clones. When the signals were not inhibited by heparin as seen in some normal gastric glands, those signals were

considered nonspecific (Figure S5D). We then evaluated the distribution of the Ags of the anti-dsGAG/NA clones in normal human tissues. Most of the tissues showed negativity in the IHC, while

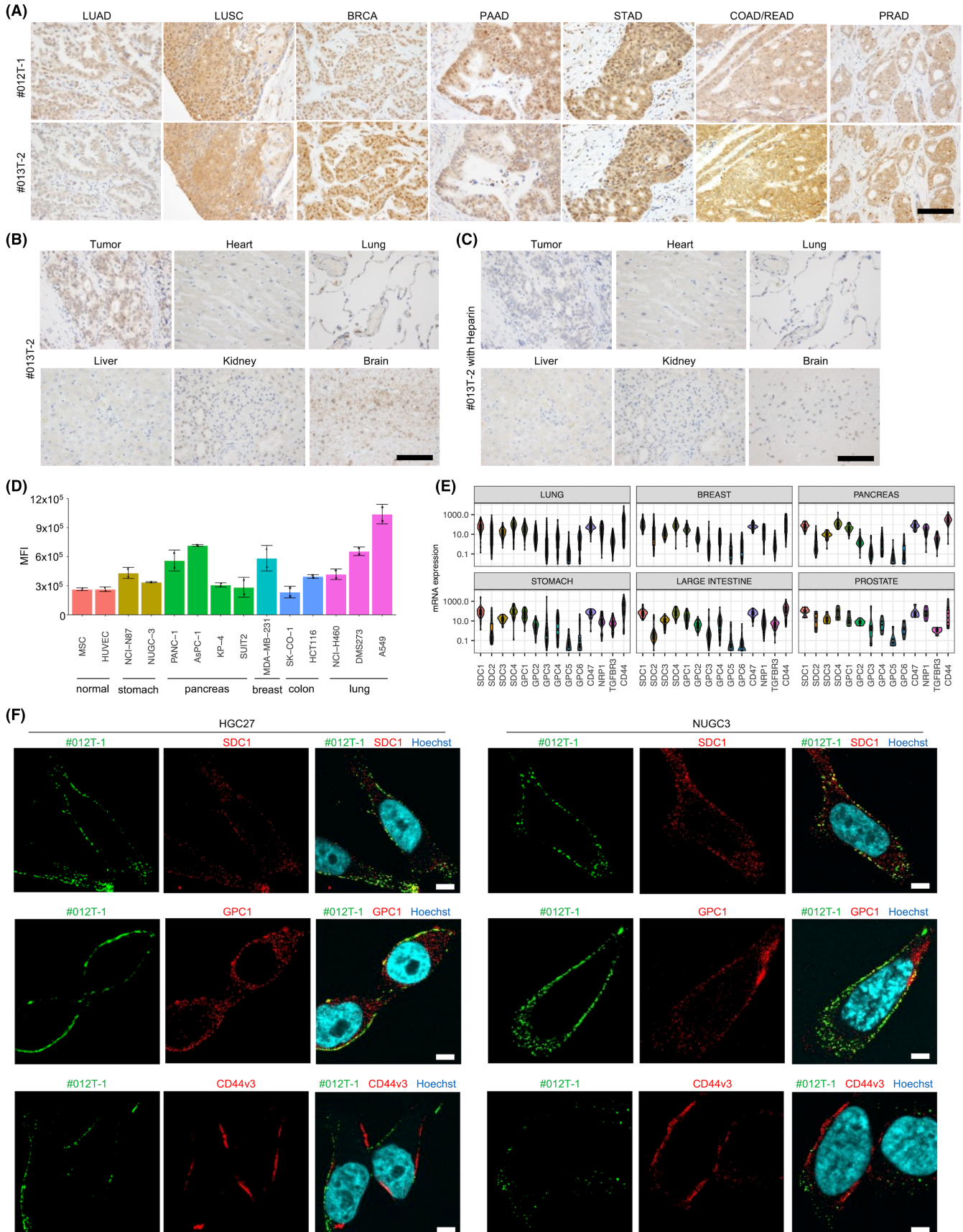


FIGURE 5 Immunohistochemical and immunocytochemical analyses of anti-densely sulfated glycosaminoglycan/nucleic acid (anti-dsGAG/NA) clones. A, Representative images of immunohistochemistry (IHC) using #012T-1 and #013T-2 for various human cancers. Scale bars indicate 100 μm . B, C, IHC of tissue microarrays containing normal human tissues using #013T-2 with/without prior coinubation of heparin. Scale bars indicate 100 μm . D, Mean fluorescent intensities (MFIs) of flow cytometry (FC) signals of various human normal and cancer cell lines using a representative high-affinity anti-dsGAG/NA clone, #022T-2 (pH 6.0) ($n = 3$). E, The mRNA expression levels of membrane heparan sulfate (HS) proteoglycans in the cancer cell line encyclopedia (CCLE) dataset. F, The immunocytochemistry (ICC) images of HGC27 and NUGC3 without permeabilization using #012T-1, together with anti-proteoglycan antibodies. Scale bars indicate 5 μm .

moderate to weak positivity was observed in brain parenchyma, pancreatic acinus, and the white pulp in the spleen (Figure 5B,C; Figure S5E). Similar results were observed in IHC using other high-affinity anti-dsGAG/NA clones, although signal intensities were weaker (Figure S5F). In FC, cell surface bindings of the anti-dsGAG/NA clones on various human cancer cells were observed, while normal human cell lines, MSC and HUVEC, exhibited lower signals (Figure 5D). It was concluded that the Ags of anti-dsGAG/NA clones exist universally in a wide spectrum of human cancer cells.

The cell surface Ags of anti-dsGAG/NA clones are considered to exist mainly as HS proteoglycans,^{20,42} among which abundant mRNA expression was observed for SDC1, SDC4, GPC1, CD47, and CD44 in cancer cell line encyclopedia (CCLE) datasets (Figure 5E). Colocalization of ICC signals of anti-dsGAG/NA clones with the five representative HS proteoglycans was investigated. The ICC signals were detected on cancer cell surfaces in a punctate manner, which were occasionally colocalized with SDC1, GPC1, and CD47, while almost no colocalizations were observed for SDC4 or CD44v3 (Figure 5F; Figure S5G). These results indicate that specific dsGAG epitopes somehow bind to specific subsets of spatially regulated HS proteoglycans. Our finding is consistent with a previous report which revealed the existence of two types of HS clusters on xenopus oocyte surface, highly and less sulfated HS, both of which were distributed in a spatially different manner on a single cell.⁴³

3.6 | Anti-dsGAG/NA Ig clones internalized rapidly into cancer cells in acidic pH

The findings on the IHC (Figure 5) indicate that the anti-dsGAG/NA clones would exhibit broad antitumor effects. It is well known that HS/heparin captures heparin-binding growth factors^{20,44}; therefore, we sought to determine whether the anti-dsGAG/NA clones inhibit these tumor-promoting functions of the dsGAG. However, neither neutralizing effects for heparin-binding growth factors (FGF7 and HB-EGF) nor inhibitions of cell invasion were observed (Figure S6A–E). Although slight growth suppressions were observed in some combinations of anti-dsGAG/NA clones and human cancer cell lines as reported previously,¹⁷ therapeutically effective levels of growth inhibitions were not achieved in our experimental settings (Figure S6F).

Antibody-dependent cellular cytotoxicity (ADCC) activity was not induced by the anti-dsGAG/NA clones in vitro (Figure S6G). Endocytosis of surface-bound Abs is one of the inhibiting factors against ADCC activity⁴⁵; thus, we hypothesized that these clones could be effectively internalized into cancer cells. It is of note that, in

an acidic condition at pH 6.0, the internalizations of the anti-dsGAG/NA clones into cancer cells were observed substantially quickly (Figure 6A). We established acidic pH-resistant cancer cell lines, called GSU-A and LLCm1A⁴⁶ (Figures S6H–L). Antibody-feeding assay in acidic pH conditions demonstrated that 30% and 60% of surface-bound anti-dsGAG/NA clones were internalized into cells in 30 and 90 minutes, respectively, at 37°C (Figures 6B–D). Lipid raft-mediated endocytosis was suggested to play a role in the internalization of the anti-dsGAG/NA clones (Figure 6E; Figure S6M). Accumulation of the internalized Abs in lysosomes was confirmed using ICC (Figure 6F). The internalization of the anti-dsGAG/NA clones was substantially quicker than that of trastuzumab (Figure 6C; Figure S6N) and comparable to that of gemtuzumab,⁴⁷ both of which are clinically applied as ADCs, in which the rapid internalization and lysosomal localization of Abs are desirable.^{47,48}

3.7 | ADC of the anti-dsGAG/NA clone showed therapeutic efficacy in vivo

The acidic pH selectivity (Figure 3) and tumor-specific reactivities (Figure 5) of the anti-dsGAG/NA clones will achieve the selective delivery of the clones to tumor tissues in vivo. When the #012T-1 anti-dsGAG/NA clone was injected into mice, the accumulation of the Ig in tumors was observed using IHC (Figures S7A,B); therefore, we proceeded to construct an ADC of an anti-dsGAG/NA clone to evaluate its therapeutic applicability and tumor-specific effects in vivo.

Initially, we constructed an ADC using #022T-2 based on its relatively high affinity and clear acidic pH selectivity among others (Figures 1–3). To obtain adequate productivity of ADC for in vivo analysis, we designed a modified form of #022T-2 (#022T-2m) without changing CDRs, which preserved the Ag specificity and acidic pH selectivity (Figure S7C–F). Eventually, a #022T-2m-based ADC was successfully constructed by conjugating maleimidocaproyl-valine-citrulline-p-aminobenzoxyloxycarbonyl-monomethyl auristatin E (MC-VC-PAB-MMAE)^{34,49} (Figure S7G). This #022T-2-based ADC, named #022T-2m-VC-PAB-MMAE, showed sub-nanomolar IC₅₀ cytotoxicity against various cancer cell lines in vitro (Figure 6G).

The Ags of the anti-dsGAG/NA clones exist commonly in both human and mouse as confirmed in FC where a mouse cell line, LLCm1A, showed positive signals (Figure 6C); therefore, these clones are suitable for testing in mouse models. The in vivo pharmacokinetics of the #022T-2m-VC-PAB-MMAE was comparable to that of trastuzumab emtansine⁵⁰ (Figure 7A), consistent with the expected low expression of the Ags in normal tissues (Figure 5). The

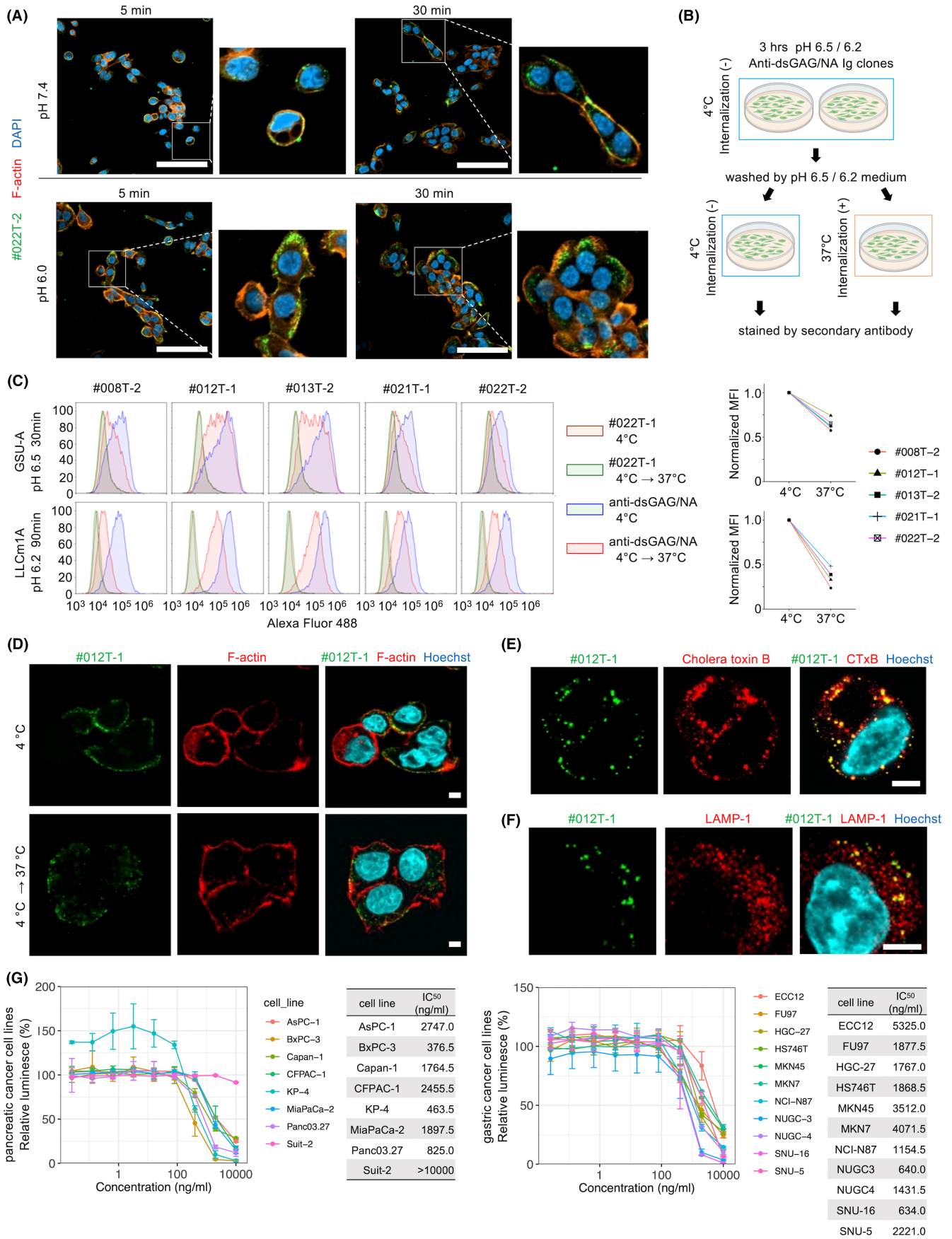


FIGURE 6 Functional properties of anti-dsGAG/NA clones for tumor cells. A, Cell surface binding and internalization of #022T-2 in pH 7.4 or 6.0 were evaluated using NUGC3 cell. Scale bars indicate 100 μm . B, Workflow of the internalization assay using acidic pH-resistant cells. C, Cell surface-bound anti-dsGAG/NA clones on GSU-A cell and LLCm1A were evaluated by flow cytometry (FC), and normalized differences of the mean fluorescent intensities (MFIs) between 4°C and 37°C are summarized in right panels. D, The internalizations of #012T-1 were assessed by immunocytochemistry (ICC) at pH 6.5. Scale bars indicate 5 μm . E, Lipid raft-mediated internalization of the anti-dsGAG/NA clone was assessed by incubating GSU-A cells with #012T-1 and fluorescent-labeled cholera toxin B (CTxB, red). Scale bar indicates 5 μm . F, Lysosomal delivery of the anti-dsGAG/NA clone (#012T-1) in GSU-A cells (pH 6.5) was evaluated by ICC using anti-LAMP1 Ab. Scale bar indicates 5 μm . G, Cytotoxicity of the #022T-2m-VC-PAB-MMAE-ADC against human pancreatic and gastric cancer cell lines. IC₅₀ value of each cell line is indicated in the table on right side.

anti-dsGAG/NA clones universally reacted to multiple types of cancer cells (Figure 5), and the acidic pH of tumor microenvironment is a universal factor in human malignancies,^{28-30,51,52} both of which motivated us to investigate the delivery and therapeutic efficacy of the ADC clone in vivo. To this end, we established multiple types of tumor xenograft models using human pancreatic cancer cell lines, Capan-1 and BxPC-3, and a human gastric cancer cell line, NUGC4, which were treated with various regimens of ADC administration (Figure 7B). In all xenograft models, the #022T-2m-VC-PAB-MMAE ADC successfully reduced the tumor sizes in any treatment regimens (Figures 7C-E). Moreover, many xenograft tumors surprisingly exhibited macroscopically complete remissions at the endpoints after 2 or 3 \times 20 mg/kg administration regimens (Figures 7C-E). Weight loss was not observed in mice under such regimens, except for the Capan-1 xenograft model under 3 \times 20 mg/kg administration regimen (Figures 7C-E). Elevations of biochemical damage markers for liver and kidney or histopathological damages in vital organs were not observed in mice under any treatment regimens in the NUGC4 xenograft model (Figure 7F,G; Figure S7H). Although reactivity of the anti-dsGAG/NA clones was mildly detected in IHC in the brain, pancreas, and spleen (Figure 5B,C; Figure S5E), neither behavioral disorders nor histological damages in the pancreas and spleen were observed. These data evidenced the extremely high efficacy of the #022T-2m-VC-PAB-MMAE ADC for multiple human cancers in vivo.

4 | DISCUSSION

One of the most interesting findings in this study is the unexpectedly less diversified acquired B cell immunity in human tumor environments. At least 60.0% (18/30) of the dominant clones identified in tumor environments of 129 human cancer cases were either anti-dsGAG/NA or anti-NA-associated proteins, both of which were associated with NAs. Those clones were considered commonly stimulated by innate immune system most likely by the TLR axis; therefore, the majority of the cancer-associated humoral immunity is presumably evoked by NAs. Furthermore, half of the dominant clones with defined Ags (10/20) commonly exhibited signature dual reactivity to the dsGAG/NA. Using the analogy with T cell immunity, where various overexpressed Ags and neo-Ags are frequently targeted,⁵³⁻⁵⁷ we and probably others would hypothesize that B cell-mediated humoral immunity also targets such cancer-related personal Ags in each case.⁵⁸ However, our data unexpectedly

clarified that such case-specific immunity for neo-Ags, although existing, might constitute a limited portion of cancer-associated humoral immunity. This surprisingly lower-than-expected diversity of the humoral Ag repertoire promotes innovative changes in the way of thinking of cancer immunity.

The emergence of anti-dsGAG/NA clones in tumor environments was considered driven by NA-induced innate immunity in B cells, consistent with the situation of tumor microenvironments where destructed and leaked NAs are abundant.⁵⁹⁻⁶¹ At the same time, high-affinity anti-dsGAG/NA clones clearly showed higher frequencies of nonsynonymous SHMs in CDRs. Thus, the intimate interplay of innate and acquired immunity plays pivotal roles in the maturation/expansion of anti-dsGAG/NA clones in tumor microenvironments. Anti-dsGAG/NA clones initially emerged through immunological stimulation by NA and were thereafter empowered with the pH-selective reactivity to the dsGAG. Such diversification or switching of epitope specificity from the initial target to another has been described as “epitope spreading” in various contexts.⁶²⁻⁶⁵ This novel type of tumor-specific epitope spreading between NAs and dsGAGs during the development of B/plasma cell clones is a key driving force of the skewed and dominant humoral immunity in tumor environments (Figure 7H).

The origin of tumor-infiltrating B/plasma cells has not been concluded to date in contrast to the tumor-infiltrating CD8 T cells, which are broadly recognized to originate from tumor-draining regional LNs (the cancer immunity cycle theory).⁶⁶⁻⁶⁸ Systematic RNA-ISH analyses and the study of the interaction between the SHMs and tTLS scores of tumors revealed that the major source of the tumor-infiltrating IgG+ B/plasma cells is tumor microenvironments, more specifically, tTLSs. Our finding is supported by recent studies showing that affinity maturation and clonal expansions of tumor-associated B cells occurred in ovarian cancer tissues⁶⁹ and in tTLS in renal cell cancers.⁹ It is rational that the tTLSs are the origins of the acidic pH-selective tumor-associated Ig clones, in which the intratumoral acidity contributes to the production and maturation of the pH-selective anti-dsGAG/NA clones. Acidic pH was previously reported to promote Ag presentation and phagocytosis of dendritic cells and macrophages,^{70,71} supporting our hypothesis that the acidic pH in tumor microenvironments is the trigger for the development of acidic pH-selective Ig clones.

The IHC analysis on clinical samples revealed that anti-dsGAG/NA clones were specifically and frequently reactive to wide ranges of human malignancies, including almost all the epithelial cancers

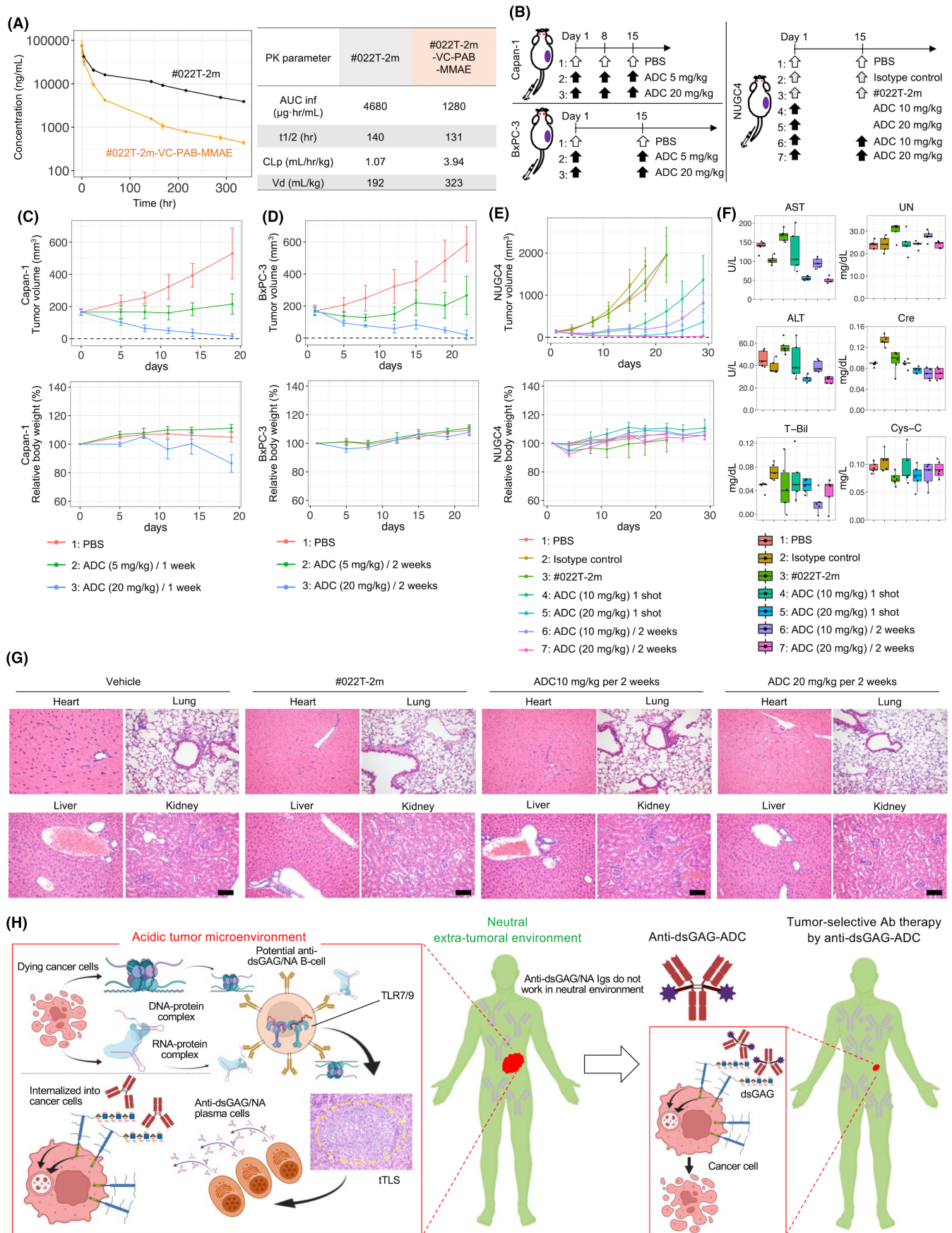


FIGURE 7 Therapeutic applicability of anti-densely sulfated glycosaminoglycan/nucleic acid (anti-dsGAG/NA) clone as an antibody-drug-conjugate (ADC) platform. A, In vivo pharmacokinetics of #022T-2m and #022T-2m-VC-PAB-MMAE ($n = 2$). B, Treatment regimens of #022T-2m-VC-PAB-MMAE-ADC. C-E, Tumor volumes and relative body weights of xenograft models of Capan-1 (C), BxPC-3 (D), and NUGC4 (E) ($n = 5$). F, Serum levels of biochemical tissue damage markers in NUGC4 xenografts ($n = 5$). G, Representative histopathological images of vital organs in NUGC4 xenograft mice treated with indicated regimens. Scale bars indicate 100 μm . H, Schematic summary of this study.

of various organs (Figure 5). Even though those high-affinity anti-dsGAG/NA clones were initially discovered in gastric cancers, this broad reactivity to various tumors would unexpectedly achieve therapeutic applicability to nearly all human cancers. Moreover, as anti-dsGAG/NA clones showed lower pH-dependently enhanced reactivities to the cellular Ags (Figure 3), it is highly likely that the in vivo reactivities of the Abs in the acidic tumor environments would substantially be manifested in clinical settings.

Acidic pH is one of the universal characteristics of tumor microenvironments and is associated with therapeutic resistance and activated tumor growth.^{29,52,72-75} In this regard, Abs with acidic pH-selective reactivity are highly demanded for cancer therapy aiming at specific intratumor delivery.^{35,36} In this study, we coincidentally found multiple pH-selective natural Abs in human tumors. We are of the opinion that broadly shared cell surface Ags of anti-dsGAG/NA clones and their pH-selective reactivity worked in concert to exert therapeutic effects in xenograft tumor models for multiple human cancers (Figure 7). The anti-dsGAG/NA clones target general common features of cancer cells and their environments, which are dsGAG/NA Ags and acidic pH (Figure 7H); therefore, they will be a "one medicine for all cancers" type therapeutic agent applicable for indifferent types of malignancies, including those with different targetable driver mutations and even those without targetable alterations.

In this study, the therapeutic applicability of anti-dsGAG/NA clones as ADC platform in multiple human cancers was clearly evidenced. A possible concern is their cross reactivity with nontumor tissues. Regarding dsGAG Ag, we revealed that dsGAGs are expressed on cancer cells of various organs, but mild positivity was also observed in a few normal tissues, such as brain (Figure 5B). Despite the immunohistochemical reactivity, physiological access of anti-dsGAG/NA Igs to the brain is negligible with the existence of blood brain barrier.⁷⁶⁻⁷⁹ In addition, ADC-treated mice did not show obvious adverse effects during the regimens in both biochemical and histopathological examinations (Figure 7F, G; Figure 57H); therefore, cross-reactivities to normal tissues should be limited. Weight loss of mice was observed under $3 \times 20\text{mg/kg}$ administration, while not under $2 \times 20\text{mg/kg}$ administration (Figure 7); therefore, in future preclinical studies, fine tuning of administration regimens would be necessary. Nonetheless, clinical applicability of the anti-dsGAG/NA clones is strongly promising because macroscopic complete remissions could be achieved under lower-dose conditions without any adverse effects (Figure 7). NAs are well-known Ags of autoimmune diseases, such as SLE.^{80,81} There are some previous reports indicating that lupus nephritis patients had Abs reactive to both GAG and NA, which could bind to glomerular basement membranes (GBM) via HS.^{82,83} It might appear

that those Abs are similar to the anti-dsGAG/NA clones in tumor environments; however, significant differences between them should be noted. The HS on GBM is mostly composed of less sulfated motifs,^{84,85} which showed apparent negativity in ELISA using tumor-associated anti-dsGAG/NA clones (Figure 1). Moreover, the IHC showed clear negativity in the GBM (Figure 5). It is concluded that the specific interactions of anti-dsGAG/NA clones with only densely sulfated forms of GAG made the clones selectively reactive to cancers.

In summary, this study clarified the unexpected paucity of Ag diversity in tumor-associated humoral immunity and revealed that the majority of intratumor Igs commonly exhibit anti-dsGAG/NA property. This defined subset of tumor-associated B cell immunity is considered to be developed through tumor-specific epitope spreading, in which anti-dsGAG/NA clones are initially stimulated by NAs and thereafter acquire additional pH-selective anti-dsGAG property. The effective in vivo therapeutic applicability of the first-in-class pH-selective anti-dsGAG/NA Igs will pave the way to fight universally against wide spectrums of cancers, even for those without targetable alterations.

ACKNOWLEDGMENTS

The authors would like to thank Ms. Miharu Tamukai and Ms. Aiko Nishimoto for their excellent office works. We are grateful to Mr. Shin Aoki for making histopathological slides. Ramos Nf-kB GFP cell is a kind gift from Dr. Kensuke Miyake, The University of Tokyo. Figure 1(A) and Figure 7(H) were created with [BioRender.com](https://www.biorender.com).

FUNDING INFORMATION

This study was supported by the AMED Science and Technology Platform Program for Advanced Biological Medicine (JP22am0401010) to S. I.; AMED Research on Development of New Drugs (JP22ak0101096), KAKENHI Grant-in-Aid for Scientific Research (A) (19H01032), and Research Grant from Mizutani Foundation for Glycoscience to H. Katoh; and research fund from Taiho Pharmaceutical Co., Ltd.

DISCLOSURE

S.S., R.H., S. Akita., H. Matsumura, A.M., C.Y., and K.M. are employees of Taiho Pharmaceutical Co., Ltd. H. Katoh and S.I. have a joint research fund from Taiho Pharmaceutical Co., Ltd. S.I. and K.A. are editorial board members of Cancer Science. Other authors have no conflicts of interest.

ETHICS STATEMENT

- Approval of the research protocol by an Institutional Reviewer Board: This study has been approved by the institutional review

boards of the University of Tokyo, Tokyo Medical and Dental University, and National Cancer Center Hospital, Tokyo, Japan.

- Informed Consent: N/A.
- Registry and the Registration No. of the study/trial: N/A.
- Animal Studies: The animal studies have been approved by Taiho Pharmaceutical Co., Ltd. and the University of Tokyo, where appropriate.

ORCID

Hiroto Katoh  <https://orcid.org/0000-0001-9440-728X>

Daisuke Komura  <https://orcid.org/0000-0002-0038-728X>

Akira Sugiyama  <https://orcid.org/0000-0003-4406-9475>

Nobuyoshi Hiraoka  <https://orcid.org/0000-0003-4215-4385>

Kazunori Aoki  <https://orcid.org/0000-0002-1292-3764>

REFERENCES

- Wei SC, Duffy CR, Allison JP. Fundamental mechanisms of immune checkpoint blockade therapy. *Cancer Discov*. 2018;8(9):1069-1086.
- Fridman WH, Petitprez F, Meylan M, et al. B cells and cancer: to B or not to B? *J Exp Med*. 2021;218(1):1-11.
- Sharonov GV, Serebrovskaya EO, Yuzhakova DV, Britanova OV, Chudakov DM. B cells, plasma cells and antibody repertoires in the tumour microenvironment. *Nat Rev Immunol*. 2020;20(5):294-307.
- Ammirante M, Luo JL, Grivennikov S, Nedospasov S, Karin M. B-cell-derived lymphotoxin promotes castration-resistant prostate cancer. *Nature*. 2010;464(7286):302-305.
- Mizoguchi A, Mizoguchi E, Takedatsu H, Blumberg RS, Bhan AK. Chronic intestinal inflammatory condition generates IL-10-producing regulatory B cell subset characterized by CD1d upregulation. *Immunity*. 2002;16(2):219-230.
- Hu X, Zhang J, Wang J, et al. Landscape of B cell immunity and related immune evasion in human cancers. *Nat Genet*. 2019;51(3):560-567.
- Cabrita R, Lauss M, Sanna A, et al. Tertiary lymphoid structures improve immunotherapy and survival in melanoma. *Nature*. 2020;577(7791):561-565.
- Helmi BA, Reddy SM, Gao J, et al. B cells and tertiary lymphoid structures promote immunotherapy response. *Nature*. 2020;577(7791):549-555.
- Meylan M, Petitprez F, Becht E, et al. Tertiary lymphoid structures generate and propagate anti-tumor antibody-producing plasma cells in renal cell cancer. *Immunity*. 2022;55(3):527-541.e5.
- Petitprez F, de Reyniès A, Keung EZ, et al. B cells are associated with survival and immunotherapy response in sarcoma. *Nature*. 2020;577(7791):556-560.
- Vanhersecke L, Brunet M, Guégan JP, et al. Mature tertiary lymphoid structures predict immune checkpoint inhibitor efficacy in solid tumors independently of PD-L1 expression. *Nat Cancer*. 2021;2(8):794-802.
- Cancro M, Carter R, Crispe I, et al. The development of B and T lymphocytes. In: Murphy K, Weaver C, eds. *Janeway's Immunobiology*. 9th ed. Garland Science; 2017:295-343.
- Sok D, Burton DR. Recent progress in broadly neutralizing antibodies to HIV. *Nat Immunol*. 2018;19(11):1179-1188.
- Garaud S, Zayakin P, Buisseret L, et al. Antigen specificity and clinical significance of IgG and IgA autoantibodies produced in situ by tumor-infiltrating B cells in breast cancer. *Front Immunol*. 2018;9(NOV):1-12.
- Pavoni E, Monteriù G, Santapaola D, et al. Tumor-infiltrating B lymphocytes as an efficient source of highly specific immunoglobulins recognizing tumor cells. *BMC Biotechnol*. 2007;7(1):70.
- Atsumi S, Katoh H, Komura D, et al. Focal adhesion ribonucleoprotein complex proteins are major humoral cancer antigens and targets in autoimmune diseases. *Commun Biol*. 2020;3(1):588.
- Katoh H, Komura D, Konishi H, et al. Immunogenetic profiling for gastric cancers identifies sulfated glycosaminoglycans as major and functional B cell antigens in human malignancies. *Cell Rep*. 2017;20(5):1073-1087.
- Lindahl U, Couchman J, Kimata K, et al. Proteoglycans and sulfated glycosaminoglycans. In: Varki A, Cummings RD, Esko JD, et al., eds. *Essentials of Glycobiology*. 3rd ed. Cold Spring Harbor Laboratory Press; 2017:207-221.
- Sasisekharan R, Shriver Z, Venkataraman G, Narayanasami U. Roles of heparan-sulphate glycosaminoglycans in cancer. *Nat Rev Cancer*. 2002;2(7):521-528.
- Sarrazin S, Lamanna WC, Esko JD. Heparan sulfate proteoglycans. *Cold Spring Harb Perspect Biol*. 2011;3(7):a004952.
- Pepi LE, Sanderson P, Stickney M, Amster IJ. Developments in mass spectrometry for glycosaminoglycan analysis: a review. *Mol Cell Proteomics*. 2021;20:100025.
- Guerrini M, Beccati D, Shriver Z, et al. Oversulfated chondroitin sulfate is a contaminant in heparin associated with adverse clinical events. *Nat Biotechnol*. 2008;26(6):669-675.
- Jones LS, Yazzie B, Middaugh CR. Polyanions and the proteome. *Mol Cell Proteomics*. 2004;3(8):746-769.
- Neuman RC. Nucleic acids. In: Neuman RC, eds. *Organic Chemistry*. University of California; 2013:1-26.
- Remko M, Broer R, Van Duijnen PT. How acidic are monomeric structural units of heparin? *Chem Phys Lett*. 2013;590:187-191.
- Junt T, Barchet W. Translating nucleic acid-sensing pathways into therapies. *Nat Rev Immunol*. 2015;15(9):529-544.
- Schlee M, Hartmann G. Discriminating self from non-self in nucleic acid sensing. *Nat Rev Immunol*. 2016;16(9):566-580.
- Kato Y, Ozawa S, Miyamoto C, et al. Acidic extracellular microenvironment and cancer. *Cancer Cell Int*. 2013;13(1):89.
- McDonald PC, Chafe SC, Brown WS, et al. Regulation of pH by carbonic anhydrase 9 mediates survival of pancreatic cancer cells with activated KRAS in response to hypoxia. *Gastroenterology*. 2019;157(3):823-837.
- Rohani N, Hao L, Alexis MS, et al. Acidification of tumor at stromal boundaries drives transcriptome alterations associated with aggressive phenotypes. *Cancer Res*. 2019;79(8):1952-1966.
- Anemone A, Consolino L, Conti L, et al. Tumour acidosis evaluated in vivo by MRI-CEST pH imaging reveals breast cancer metastatic potential. *Br J Cancer*. 2021;124(1):207-216.
- Böhme I, Bosserhoff AK. Acidic tumor microenvironment in human melanoma. *Pigment Cell Melanoma Res*. 2016;29(5):508-523.
- Reshetnyak YK. Imaging tumor acidity: pH-low insertion peptide probe for optoacoustic tomography. *Clin Cancer Res*. 2015;21(20):4502-4504.
- Kang JC, Sun W, Khare P, et al. Engineering a HER2-specific antibody-drug conjugate to increase lysosomal delivery and therapeutic efficacy. *Nat Biotechnol*. 2019;37(5):523-526.
- Johnston RJ, Su LJ, Pinckney J, et al. VISTA is an acidic pH-selective ligand for PSGL-1. *Nature*. 2019;574(7779):565-570.
- Chang HW, Frey G, Liu H, et al. Generating tumor-selective conditionally active biologic anti-CTLA4 antibodies via protein-associated chemical switches. *Proc Natl Acad Sci*. 2021;118(9):1-10.
- Igawa T, Ishii S, Tachibana T, et al. Antibody recycling by engineered pH-dependent antigen binding improves the duration of antigen neutralization. *Nat Biotechnol*. 2010;28(11):1203-1207.
- Sulea T, Rohani N, Baardnes J, et al. Structure-based engineering of pH-dependent antibody binding for selective targeting of solid-tumor microenvironment. *MAbs*. 2020;12(1):1682866.
- Bohannon C, Powers R, Satyabhaman L, et al. Long-lived antigen-induced IgM plasma cells demonstrate somatic mutations and contribute to long-term protection. *Nat Commun*. 2016;7(1):11826.

40. Hou B, Saudan P, Ott G, et al. Selective utilization of toll-like receptor and MyD88 signaling in B cells for enhancement of the antiviral germinal center response. *Immunity*. 2011;34(3):375-384.
41. Hua Z, Gross AJ, Lamagna C, et al. Requirement for MyD88 signaling in B cells and dendritic cells for germinal center anti-nuclear antibody production in Lyn-deficient mice. *J Immunol*. 2014;192(3):875-885.
42. Weiss RJ, Spahn PN, Toledo AG, et al. ZNF263 is a transcriptional regulator of heparin and heparan sulfate biosynthesis. *Proc Natl Acad Sci*. 2020;117(17):9311-9317.
43. Mii Y, Yamamoto T, Takada R, et al. Roles of two types of heparan sulfate clusters in Wnt distribution and signaling in xenopus. *Nat Commun*. 2017;8(1):1973.
44. Weiss RJ, Spahn PN, Chiang AWT, et al. Genome-wide screens uncover KDM2B as a modifier of protein binding to heparan sulfate. *Nat Chem Biol*. 2021 Jun 12;17(6):684-692.
45. Chew HY, De Lima PO, Gonzalez Cruz JL, et al. Endocytosis inhibition in humans to improve responses to ADCC-mediating antibodies. *Cell*. 2020 Mar;180(5):895-914.e27.
46. Sutoo S, Maeda T, Suzuki A, Kato Y. Adaptation to chronic acidic extracellular pH elicits a sustained increase in lung cancer cell invasion and metastasis. *Clin Exp Metastasis*. 2020 Feb 5;37(1):133-144.
47. Walter RB, Raden BW, Kamikura DM, Cooper JA, Bernstein ID. Influence of CD33 expression levels and ITIM-dependent internalization on gemtuzumab ozogamicin-induced cytotoxicity. *Blood*. 2005 Feb 1;105(3):1295-1302.
48. Li JY, Perry SR, Muniz-Medina V, et al. A Biparatopic HER2-targeting antibody-drug conjugate induces tumor regression in primary models refractory to or ineligible for HER2-targeted therapy. *Cancer Cell*. 2016 Jan;29(1):117-129.
49. Khongorzul P, Ling CJ, Khan FU, Ihsan AU, Zhang J. Antibody-drug conjugates: a comprehensive review. *Mol Cancer Res*. 2020;18(1):3-19.
50. Jumbe NL, Xin Y, Leipold DD, et al. Modeling the efficacy of trastuzumab-DM1, an antibody drug conjugate, in mice. *J Pharmacokinetic Pharmacodyn*. 2010;37(3):221-242.
51. Gillies RJ, Raghunand N, Karczmar GS, Bhujwala ZM. MRI of the tumor microenvironment. *J Magn Reson Imaging*. 2002;16(4):430-450.
52. Huber V, Camisaschi C, Berzi A, et al. Cancer acidity: an ultimate frontier of tumor immune escape and a novel target of immunomodulation. *Semin Cancer Biol*. 2017;43:74-89.
53. Ahmadzadeh M, Pasetto A, Jia L, et al. Tumor-infiltrating human CD4+ regulatory T cells display a distinct TCR repertoire and exhibit tumor and neoantigen reactivity. *Sci Immunol*. 2019;4(31):eaao4310.
54. Li B, Li T, Pignon JC, et al. Landscape of tumor-infiltrating T cell repertoire of human cancers. *Nat Genet*. 2016;48(7):725-732.
55. Pasetto A, Gros A, Robbins PF, et al. Tumor- and neoantigen-reactive T-cell receptors can be identified based on their frequency in fresh tumor. *Cancer Immunol Res*. 2016;4(9):734-743.
56. Verdegaal EME, de Miranda NFCC, Visser M, et al. Neoantigen landscape dynamics during human melanoma-T cell interactions. *Nature*. 2016;536(7614):91-95.
57. Yamamoto TN, Kishton RJ, Restifo NP. Developing neoantigen-targeted T cell-based treatments for solid tumors. *Nat Med*. 2019;25(10):1488-1499.
58. Cui C, Wang J, Fagerberg E, et al. Neoantigen-driven B cell and CD4 T follicular helper cell collaboration promotes anti-tumor CD8 T cell responses. *Cell*. 2021;184(25):6101-6118.e13.
59. Jahr S, Hentze H, Englisch S, et al. DNA fragments in the blood plasma of cancer patients: quantitations and evidence for their origin from apoptotic and necrotic cells. *Cancer Res*. 2001;61(4):1659-1665.
60. Schwarzenbach H, Hoon DSB, Pantel K. Cell-free nucleic acids as biomarkers in cancer patients. *Nat Rev Cancer*. 2011;11(6):426-437.
61. Strauss J, Heery CR, Kim JW, et al. First-in-human phase I trial of a tumor-targeted cytokine (NHS-IL12) in subjects with metastatic solid tumors. *Clin Cancer Res*. 2019;25(1):99-109.
62. Brossart P. The role of antigen spreading in the efficacy of immunotherapies. *Clin Cancer Res*. 2020;26(17):4442-4447.
63. Cornaby C, Gibbons L, Mayhew V, Sloan CS, Welling A, Poole BD. B cell epitope spreading: mechanisms and contribution to autoimmune diseases. *Immunol Lett*. 2015;163(1):56-68.
64. Lehmann PV, Forsthuber T, Miller A, Sercarz EE. Spreading of T-cell autoimmunity to cryptic determinants of an autoantigen. *Nature*. 1992;358(6382):155-157.
65. Vanderlugt CL, Miller SD. Epitope spreading in immune-mediated diseases: implications for immunotherapy. *Nat Rev Immunol*. 2002;2(2):85-95.
66. Chen DS, Mellman I. Oncology meets immunology: the cancer-immunity cycle. *Immunity*. 2013;39(1):1-10.
67. Gardner A, Ruffell B. Dendritic cells and cancer immunity. *Trends Immunol*. 2016;37(12):855-865.
68. Manieri NA, Chiang EY, Grogan JL. TIGIT: a key inhibitor of the cancer immunity cycle. *Trends Immunol*. 2017;38(1):20-28.
69. Mazor RD, Nathan N, Gilboa A, et al. Tumor-reactive antibodies evolve from non-binding and autoreactive precursors. *Cell*. 2022;185(7):1208-1222.e21.
70. Tong J, Wu WN, Kong X, et al. Acid-sensing ion channels contribute to the effect of acidosis on the function of dendritic cells. *J Immunol*. 2011;186(6):3686-3692.
71. Vermeulen M, Giordano M, Trevani AS, et al. Acidosis improves uptake of antigens and MHC class I-restricted presentation by dendritic cells. *J Immunol*. 2004;172(5):3196-3204.
72. Shukla SK, Purohit V, Mehla K, et al. MUC1 and HIF-1alpha signaling crosstalk induces anabolic glucose metabolism to impart gemcitabine resistance to pancreatic cancer. *Cancer Cell*. 2017;32(1):71-87.e7.
73. Bader JE, Voss K, Rathmell JC. Targeting metabolism to improve the tumor microenvironment for cancer immunotherapy. *Mol Cell*. 2020;78(6):1019-1033.
74. Chen Q, Liu G, Liu S, et al. Remodeling the tumor microenvironment with emerging nanotherapeutics. *Trends Pharmacol Sci*. 2018;39(1):59-74.
75. Stylianopoulos T, Munn LL, Jain RK. Reengineering the tumor vasculature: improving drug delivery and efficacy. *Trends in Cancer*. 2018;4(4):258-259.
76. Chang AJ, DeSilva R, Jain S, Lears K, Rogers B, Lapi S. 89Zr-radiolabeled trastuzumab imaging in orthotopic and metastatic breast tumors. *Pharmaceuticals*. 2012;5(1):79-93.
77. Natarajan A, Zhang H, Ye W, et al. A humanized anti-GPC3 antibody for Immuno-positron emission tomography imaging of orthotopic mouse model of patient-derived hepatocellular carcinoma xenografts. *Cancers (Basel)*. 2021;13(16):3977.
78. Rousseau C, Ruellan AL, Bernardeau K, et al. Syndecan-1 antigen, a promising new target for triple-negative breast cancer immunopET and radioimmunotherapy. A preclinical study on MDA-MB-468 xenograft tumors. *EJNMMI Res*. 2011;1(1):20.
79. Chen HC, Chang HT, Huang PH, et al. Molecular imaging of heparan sulfate expression with radiolabeled recombinant eosinophil cationic protein predicts allergic lung inflammation in a mouse model for asthma. *J Nucl Med*. 2013;54(5):793-800.
80. Crispin JC, Liossis SNC, Kis-Toth K, et al. Pathogenesis of human systemic lupus erythematosus: recent advances. *Trends Mol Med*. 2010;16(2):47-57.
81. Fillatreau S, Manfroi B, Dörner T. Toll-like receptor signalling in B cells during systemic lupus erythematosus. *Nat Rev Rheumatol*. 2021;17(2):98-108.
82. Faaber P, Rijke TPM, van de Putte LBA, et al. Cross-reactivity of human and murine anti-DNA antibodies with heparan sulfate. The major glycosaminoglycan in glomerular basement membranes. *J Clin Invest*. 1986;77(6):1824-1830.
83. Krishnan MR, Wang C, Marion TN. Anti-DNA autoantibodies initiate experimental lupus nephritis by binding directly to the glomerular basement membrane in mice. *Kidney Int*. 2012;82(2):184-192.

84. Ledin J, Staatz W, Li JP, et al. Heparan sulfate structure in mice with genetically modified heparan sulfate production. *J Biol Chem.* 2004;279(41):42732-42741.
85. Wang Z, Arnold K, Xu Y, et al. Quantitative analysis of heparan sulfate using isotopically labeled calibrants. *Commun Biol.* 2020;3(1):425.

SUPPORTING INFORMATION

Additional supporting information can be found online in the Supporting Information section at the end of this article.

How to cite this article: Furuya G, Katoh H, Atsumi S, et al. Nucleic acid-triggered tumoral immunity propagates pH-selective therapeutic antibodies through tumor-driven epitope spreading. *Cancer Sci.* 2023;114:321-338. doi: [10.1111/cas.15596](https://doi.org/10.1111/cas.15596)